JOURNAL OF GEOPHYSICAL RESEARCH, VOL. 103, NO. B4, PAGES 7121–7136, APRIL 10, 1998

A regionalized upper mantle (RUM) seismic model

Ólafur Gudmundsson and Malcolm Sambridge[1]
Research School of Earth Sciences, Australian National University, Canberra

Abstract. Seismic velocity heterogeneity in the Earth's mantle is strongly concentrated near its top. The shallow heterogeneity of the mantle correlates strongly with surface tectonics. We use these observations as constraints of a tomographic experiment aimed at building a regionalized upper mantle (RUM) reference model. We use a select set of teleseismic travel times to minimize the mapping of mislocation into structure. The data selection emphasizes the robustness of individual picks. The form of the RUM model is a set of velocity profiles as functions of depth through the upper mantle for each of the different tectonic provinces of Earth. Together the profiles constitute a three-dimensional model which incorporates considerable structural detail but is described by only 90 parameters and has only about 22 degrees of freedom. This is achieved by irregularly sampling a detailed regionalization of the globe, by detailed mapping of subducted lithosphere in the mantle as defined by seismicity, and by combining these structures in an irregular grid in which bookkeeping is efficiently handled. The resulting RUM model includes subducting slabs as sharp fast features in the upper mantle. Old continents are fast; young oceans are slow. Models have been derived for both compressional and shear velocity. The RUM model is designed to represent as much of upper mantle heterogeneity as seen by body wave travel times as possible with a simple model. It can be useful as a reference model for individual tectonic regions. Travel times are efficiently generated for the RUM model. Mislocations of explosions of known location are significantly reduced when corrections for the RUM model are applied to travel time residuals for a spherically symmetrical Earth model.

1. Introduction

Global models of seismic velocity heterogeneity have emerged in the past decade which show significant deviations from spherical symmetry in Earth's structure. Most of the models for the upper mantle are primarily derived from surface waves and yield information about shear velocity structure [e.g., *Woodhouse and Dziewonski,* 1984; *Zhang and Tanimoto,* 1993]. As the quality of data and their coverage increases, more detail is included in the models. Global models currently claim to resolve structures as small as 1000 km in lateral extent [*Zhang and Lay,* 1996], although some authors give a more conservative resolution estimate [*Trampert and Woodhouse,* 1995]. Regional models, on the other hand, resolve structures to considerably smaller scales, i.e., hundreds of kilometers [e.g., *Zielhuis and Nolet,* 1994; *Debayle and Leveque,* 1997]. The strength of heterogeneity in the models increases as more detail is included. The global model RG5.5 of *Zhang and Tanimoto* [1993] has about ±3% variation at 110 km depth, while the regional model of *Zielhuis and Nolet* [1994] has about ±6% variation at the same depth.

The strength of heterogeneity in global models falls off rapidly below a few hundred kilometers depth. Typically, the heterogeneity is ±3% around 100 km depth but less than ±1% in the transition zone. Using travel times, which potentially offer higher resolution, *Gudmundsson et al.* [1990] found that the level of heterogeneity at large and intermediate scales (scale >400 km) drops by about a factor of 2 at a depth of 300 km. They also concluded that smaller-scale heterogeneity is concentrated even more strongly near the Earth's surface.

One important source of information about the structure of the upper mantle is regional refraction profiles (of length > 2500 km) and body wave travel times and waveforms from earthquakes which can be aligned along a profile of comparable length and interpreted as a refraction profile [e.g., *Helmberger and Wiggins,* 1971; *Grand and Helmberger,* 1984; *Walck,* 1984; *Mechie et al.,* 1993; *Kennett et al.,* 1994]. A comprehensive summary of the one-dimensional models which result from this approach is given by *Nolet et al.* [1994]. After comparing a large number of models from varied tectonic environments they conclude that there is clear evidence

[1]Also at Centre for Information Science Research, Australian National University.

Paper number 97JB02488.
0148-0227/98/97JB-02488$09.00

for lateral heterogeneity which correlates with surface tectonics. The model differences persist to 300-400 km depth. They also point out that local studies generally produce larger velocity anomalies than are found in global surface wave models. This suggests that global models provide only a partially complete picture of the upper mantle, with intermediate-scale features filtered out and larger-scale features damped.

Regional tomography based on travel times has revealed important aspects of subducted slab structures in the mantle [e.g., *Spakman et al.*, 1988; *Zhou and Clayton*, 1990; *van der Hilst et al.*, 1991; *Zhao et al.*, 1992]. Slabs appear as fast anomalies which display a variation of morphology, particularly at depth. In some instances, evidence for necking and detachment is seen, and some slabs appear to be driven through the phase transition at 660 km depth, while others pile up in the transition zone. While it is clear that slab morphology is complex, some of the conclusions from regional delay time tomography would be strengthened by rigorous hypothesis testing. The most reliable slab images are based on compressional waves. The strength of the anomalies for compressional velocity is as high as $\pm 5\%$, fast velocities defining the slab while the slower velocities are generally found in the shallow mantle wedge.

The picture that has emerged of the upper mantle has shear velocity vary by $\pm 3\%$ on large scales (> 1000 km) and another $\pm 3\%$ on intermediate scales (400-1000 km). Significant heterogeneity persists at smaller scales. Variations of compressional velocity are less well known but are probably comparable, while somewhat less than the variations of shear velocity. Subducting lithosphere possesses an anomaly of about 5%. Clearly, such strong heterogeneity will significantly affect the travel times of body wave phases, including those most commonly used in earthquake location. Accounting for the effect of lateral heterogeneity can therefore significantly improve the quality of event location. *Fujita et al.* [1981] estimate that the structure of a slab may affect the location of earthquakes within it by as much as 40 km. For teleseismic P waves, that translates into a time effect of about 4 s.

It is evident from even the first generation of global models and from a comparison of early one-dimensional models from different tectonic regions that the large-scale features of shallow upper mantle structure correlate well with surface tectonics [*Romanowicz*, 1991; *Nolet et al.*, 1994]. Old continental cores have deep fast roots extending into the upper mantle, and spreading centers are underlain by slow mantle rocks, although the depth extent is subject to debate. *Nataf and Ricard* [1996] attach much significance to the correlation of tomographic models for the upper mantle with surface tectonics when they suggest a velocity model (3SMAC) for the upper mantle based on a tectonic, crustal thickness and sedimentary thickness regionalization, geophysical modeling, and constraints from other fields of earth sciences than seismology. Their approach is justified by *Ricard et al.* [1996], who show that the 3SMAC model accounts well for normal-mode frequencies and phase-velocity observations worldwide.

Like *Nataf and Ricard* [1996], we regard the strong correlation of surface tectonics and velocity heterogeneity at shallow depths in the mantle, where the heterogeneity is strongest, as a potential constraint on global tomography. In this paper we apply a regionalization as a constraint to upper mantle structure derived from travel times. We seek a simple model (few model parameters) to account for as much of upper mantle heterogeneity as possible. Our objective is to build a regionalized reference model for travel time corrections.

2. Strategy

Accounting for the effects of velocity heterogeneity on travel times and thus event location must include the main features of the velocity structure and remain a simple procedure in order to be efficient. We attempt to meet these prerequisites with the following strategy:

We use the high level of correlation of global velocity models with surface tectonics to define the main features of Earth structure. A detailed regionalization defines irregularly shaped bodies on the Earth's surface which in turn define discrete model parameters. With irregular sampling of the regionalization we can represent irregular bodies with a large range of length scales. The sampling is dense where needed (i.e., at continental margins, at island arcs, and within tectonic continents) and sparse elsewhere (e.g., intraregional, oceanic).

Delaunay and Voronoi tesselation are recipes for connecting nodes in an irregular grid. In both cases the tesselation is uniquely defined and automatically generated given an arbitrary set of nodes. The Delaunay tesselation generates a space-filling set of tetrahedra with nodes at their vertices. The Voronoi tesselation defines a polyhedron around each node with faces on the median bisectors between the node in question and its natural neighbors [*Okabe et al.*, 1992]. Delaunay tetrahedra are suitable to define the volume of an object which surface has been sampled. Voronoi polyhedra are suitable to define the volume associated with a discrete sample of a varying field. We use a combination of a Delaunay tesselation and a Voronoi tesselation to define discrete regions belonging to the various tectonic types [*Sambridge and Gudmundsson*, 1998]. This allows us to significantly reduce the number of parameters needed to represent the complex regions compared to a regular grid for example. Efficient algorithms are available for navigation and book keeping in irregular grids composed of Delaunay tetrahedra or three-dimensional Voronoi cells [*Sambridge et al.*, 1995].

We use a select data set of travel times from well-located events and nuclear explosions in order to alleviate the mapping of mislocation into structure. We invert these data for an irregularly parameterized, regionalized upper mantle (RUM) model. Our objective is not to find the best possible model but to find the simplest model that still contains enough information about structure to be useful for generating corrections to travel times used in event location. Teleseismic travel times can then be corrected for this model by a relatively simple and efficient ray-tracing procedure.

3. Method

3.1. Regionalization

Figure 1 shows the regionalization. It is based on maps published by *Sclater et al.* [1980] and on *Jordan's* [1981] GRT1 regionalization. Eight tectonic regions are defined. The ocean is divided into three age provinces, the same as the GRT1 regionalization, except at a resolution of 2° compared to 5° in GRT1. The continents are divided into five regions according to age, four regions of low volcanic and earthquake activity, in addition to a region termed tectonic continent where seismic and volcanic activity is high. We have termed the regions young continent, intermediate-age continent, old continent and ancient continent as their separation in time does not strictly correspond to boundaries between geological eras. The age boundaries are listed in Figure 1 and were selected by comparing the age zonation of the continents with tomographic images of the upper mantle [e.g., *Woodhouse and Dziewonski,* 1984]. The regionalization is very similar to the regionalization used by *Nataf and Ricard* [1996] to generate the 3SMAC model. We have perhaps unconventionally termed the Iceland-Faeroe-Greenland Ridge continental because of its highly anomalous crustal thickness for oceanic crust (25-35 km according to *Bott and Gunnarsson* [1980]. We have also defined the ridges of the Tasman Sea as continental. A future improvement of the regionalization would include all oceanic ridges and plateaus as a separate oceanic region(s). This regionalization has obvious limitations. Parts of the age mapping involve significant interpolation of geochronological data. Details are left out where limited by the resolution. For the purposes of global seismology, much more detail is not justified because teleseismic delay times or surface wave dispersion will not be able to resolve it.

The regionalization is initially represented by 16,200 parameters. Roughly a quarter of these are then selected to parameterize the boundaries between the regions (4100 parameters) (see Figure 1b). The boundaries are all parameterized with a 2° resolution except the boundaries between oceanic regions. Thus the density of parameterization is high where we expect potentially sharp contrasts, i.e., at continental margins and boundaries between tectonic and atectonic regions, and low where we do not, i.e., within the oceans. Figure 1b shows the boundaries of the Voronoi cells around the selected samples of the regionalization. Figure 1b contains about 4100 Voronoi cells. Figure 1c shows how the original regionalization is reproduced by the 4100 selected cells. The full complexity of Figure 1a is reproduced in Figure 1c with only about a quarter of the number of parameters in the original. Each Voronoi cell is taken to encompass a region of uniform velocity

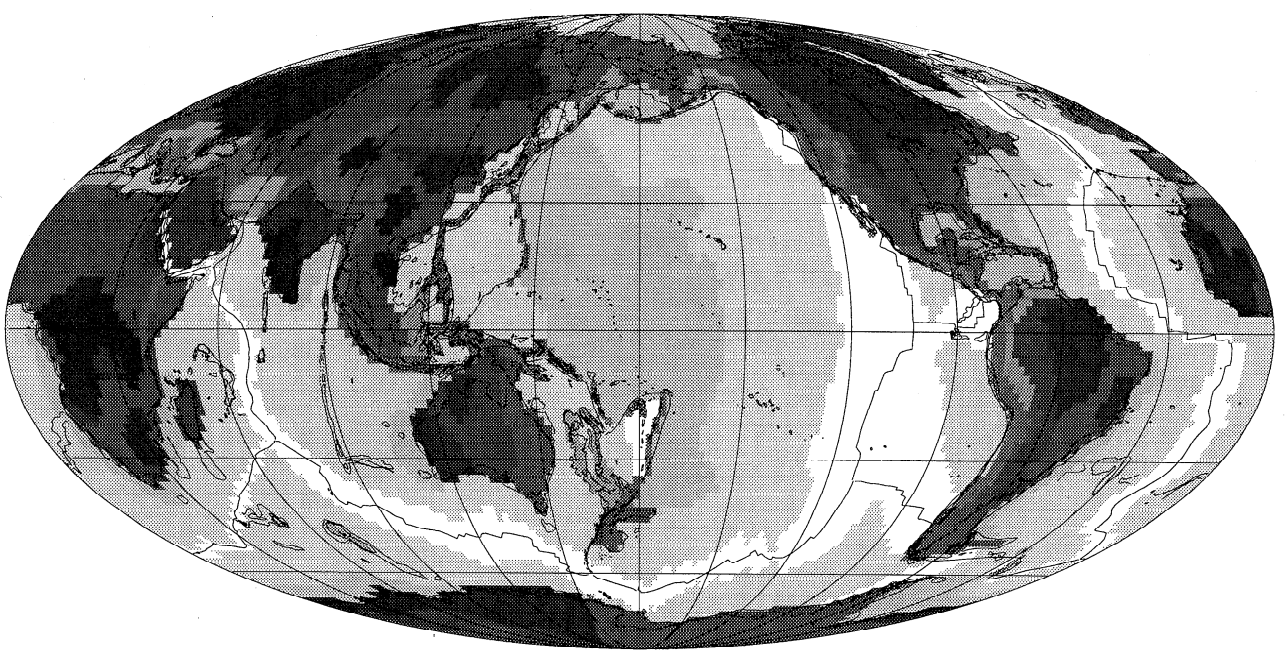

Figure 1a. Tectonic regionalization as designed on a 2x2 degree grid using 16,200 parameters.

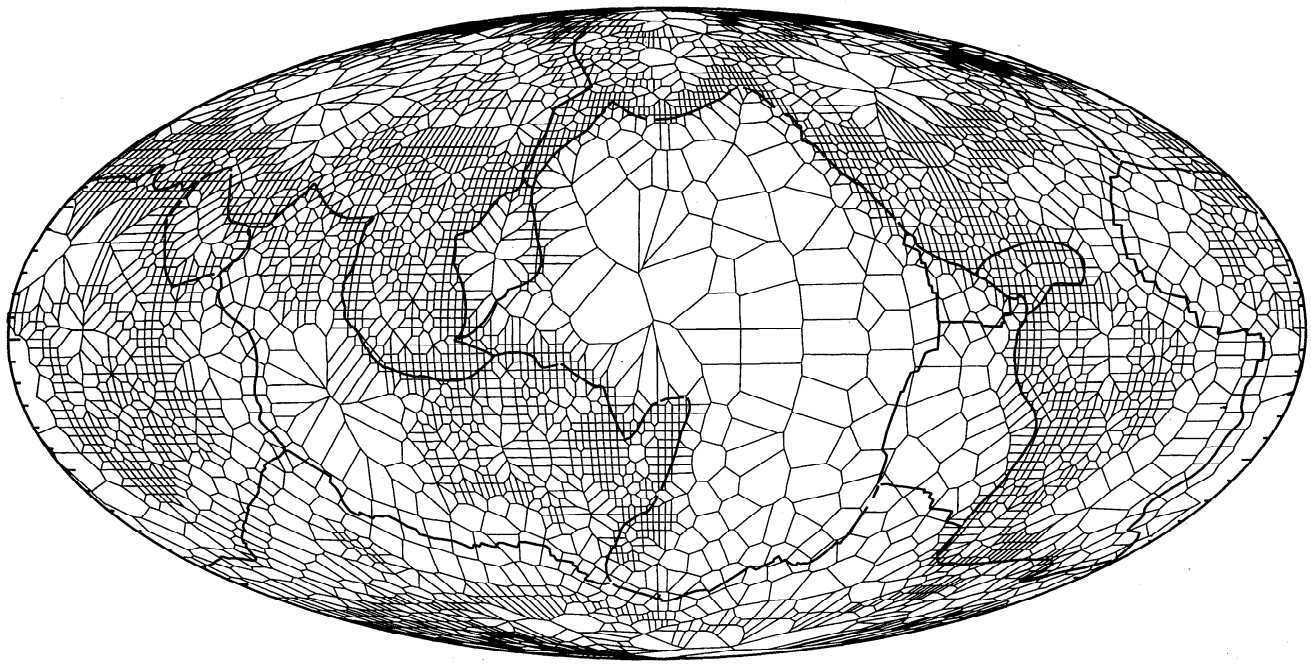

Figure 1b. Boundaries of Voronoi cells around 4100 of the original 16,200 2x2 degree cells selected to sample the details of the regionalization.

at each depth. The regionalization is extended from the surface to a depth of 660 km to span the whole of the upper mantle.

This regionalization is not taken to be a complete description of velocity heterogeneity. We ignore lower mantle heterogeneity because extrapolation of surface tectonics into the lower mantle would not be warranted and because the strength of heterogeneity decays rapidly with depth in the upper mantle. Shallow small-scale structure internal to tectonic regions is not accounted for by this regionalization. In island arc regions, such structures are modeled as subducting slabs. In continental regions, such structures are accounted for by station corrections.

The ability to reduce 16,200 parameters to 4100 is not crucial to the feasibility of the present study. However, it demonstrates conceptually a capacity to reduce computational needs which may become important once

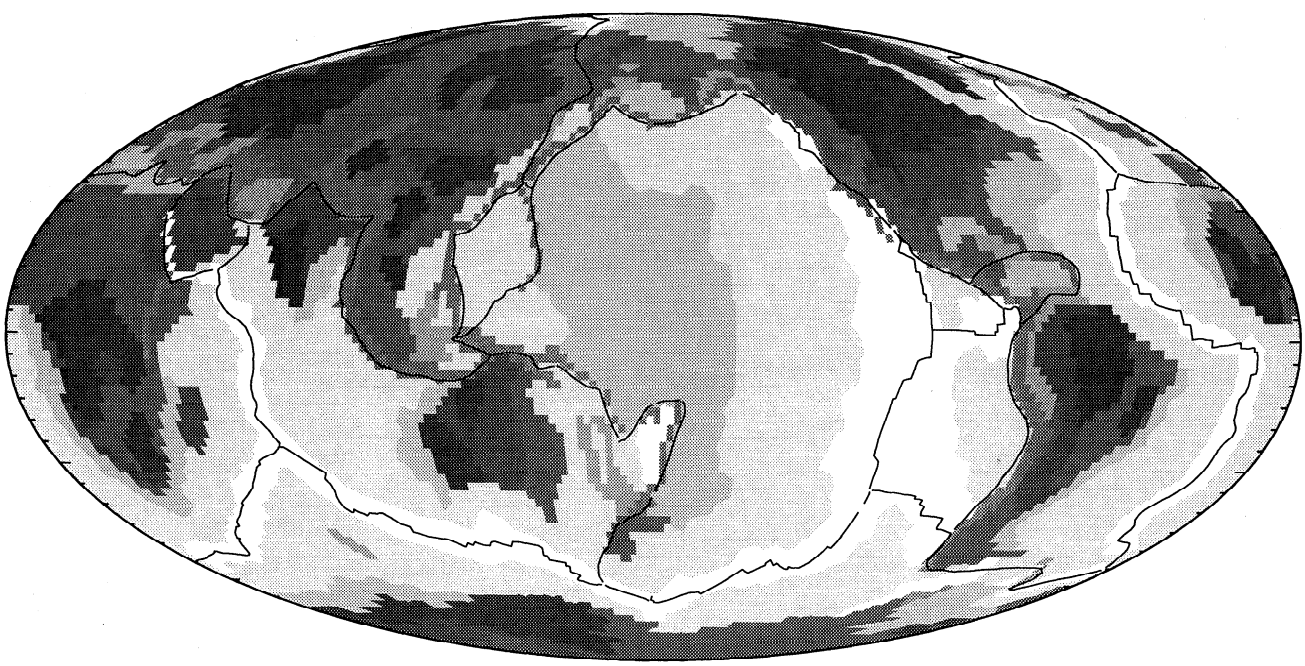

Figure 1c. The tectonic regionalization as represented by the 4100 Voronoi cells in Figure 1b.

more detail is built into the regionalization. The irregular parameterization of slab structures (section 3.2) is essential on the other hand in order to avoid an unmanageable parameterization.

3.2. Subducting Slabs

Subducting slabs are significant structures in the upper mantle which are clearly oblique and cannot be included in a two-dimensional regionalization as above. Most of Earth's seismicity occurs in or around subducting slabs. Slabs do affect travel times significantly, and their presence can, if not accounted for, cause a systematic mislocation of island-arc earthquakes by as much as 40 km [*Fujita et al.*, 1981]. We have included oblique slab structures in our parameterization of the upper mantle as the ninth region. First, we contoured slab-related seismicity world wide. A total of 24 separate slab bodies were defined (see Figure 2a). Examples of slab contours are presented in Figure 2b for the slabs of the northwest Pacific. The contours are drawn at 50 km depth intervals such that they lie near the top of the seismogenic region. We used the relocated catalog of Engdahl et al. (submitted manuscript, 1997) as well as a filtered version of the International Seismological Centre catalog (based on location quality) to define the seismicity. Neither catalog is complete, and both contain significant gaps which are difficult to interpret. These gaps were not interpolated if they exceed a few hundred kilometers in size. The slab contours obviously do not define a slab where there is no seismicity. It is difficult to envisage the thermal anomaly of subducting lithosphere to terminate as abruptly as the seismicity in many places. Thus our model of slabs is likely to be incomplete. However, slabs are defined where we most need them, i.e., where the earthquakes occur and for which travel time corrections are needed.

The slab contours define a surface which we take to define the top of the slab (or what used to be the top of the oceanic lithosphere before subduction). We then define a complimentary surface assuming that the slab is 200 km thick. This is a simplification of slab geometry, particularly at depth. No necking or slab detachment is allowed for, while it is possible that that type of morphology is associated with gaps in seismicity [*Spakman et al.*, 1998; *Widiyantoro and van der Hilst*, 1996]. Slabs are not allowed to pile up in the transition zone as appears to be the case for, e.g., the Izu-Bonin slab [*van der Hilst et al.*, 1993].

Projecting the original surface 200 km along its local normal occasionally results in the folding of the original surface. Such folds were simply edited out interactively with a graphics tool. We sample the contours using nodes placed at a lateral spacing of about 10 km. These nodes are not internal to the slabs as we define them but are on their surface. In this case, constant-velocity Voronoi cells as were used in the surface parameterization are not suitable to describe their complex geometry because these cells surround each node and would necessarily extend the slab and change its volume. Instead, we place the nodes of the slabs in a global coordinate system and construct the three-dimensional Delaunay tesselation for the approximately 23,000 slab samples for all 24 individual slab structures. Those Delaunay tetrahedra which join the two surfaces of the same slab structure then define the volume of slabs in the upper mantle. The Delaunay tetrahedral representation of the slabs of the northwest Pacific is shown in perspective in Figure 2c as an example. These are some of the larger and deeper slabs which display significant complexity in shape.

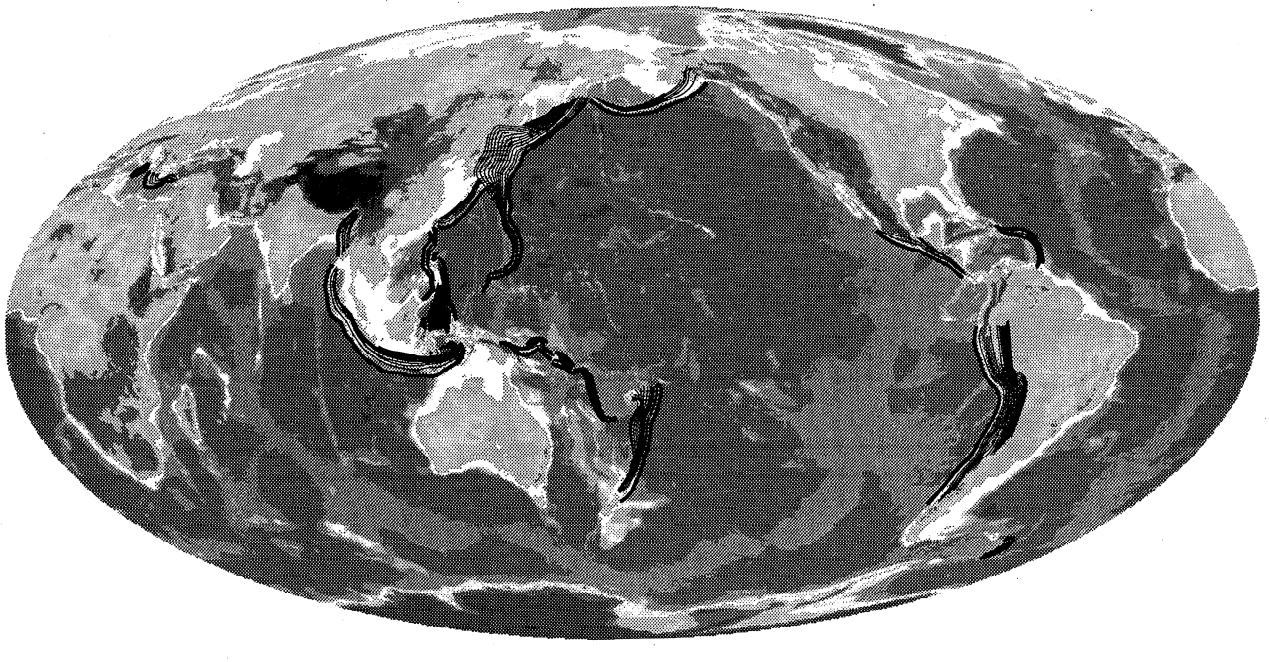

Figure 2a. Contoured subducting slabs with a topographic/bathymetric map shown for reference. The contours are at 50 km intervals in depth

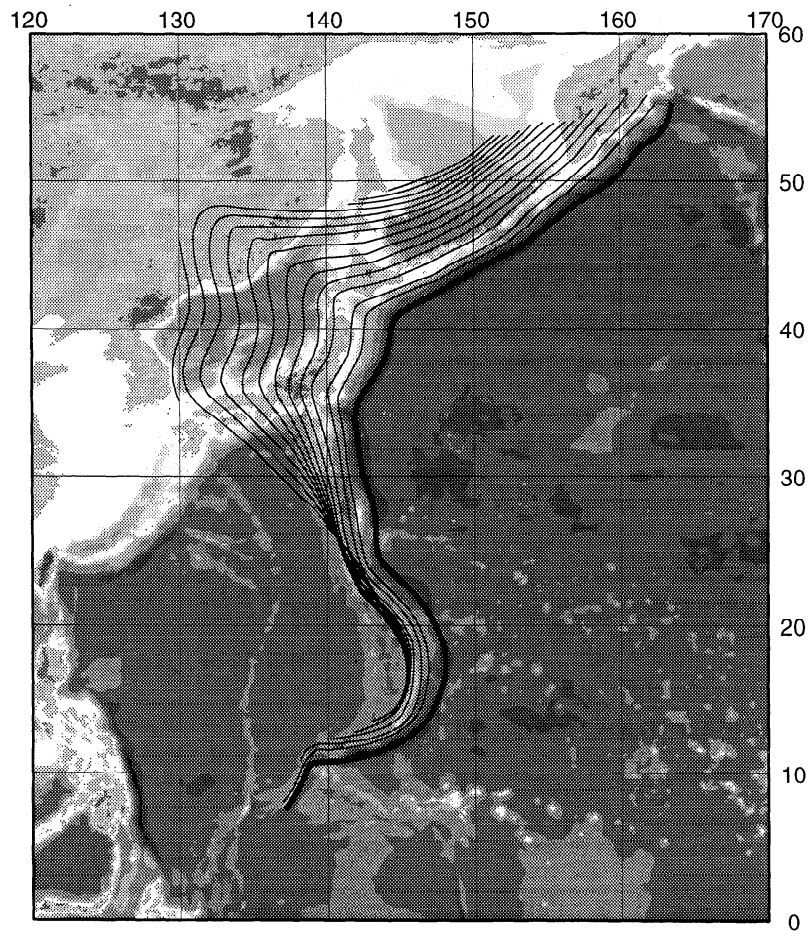

Figure 2b. The slabs of the northwest Pacific.

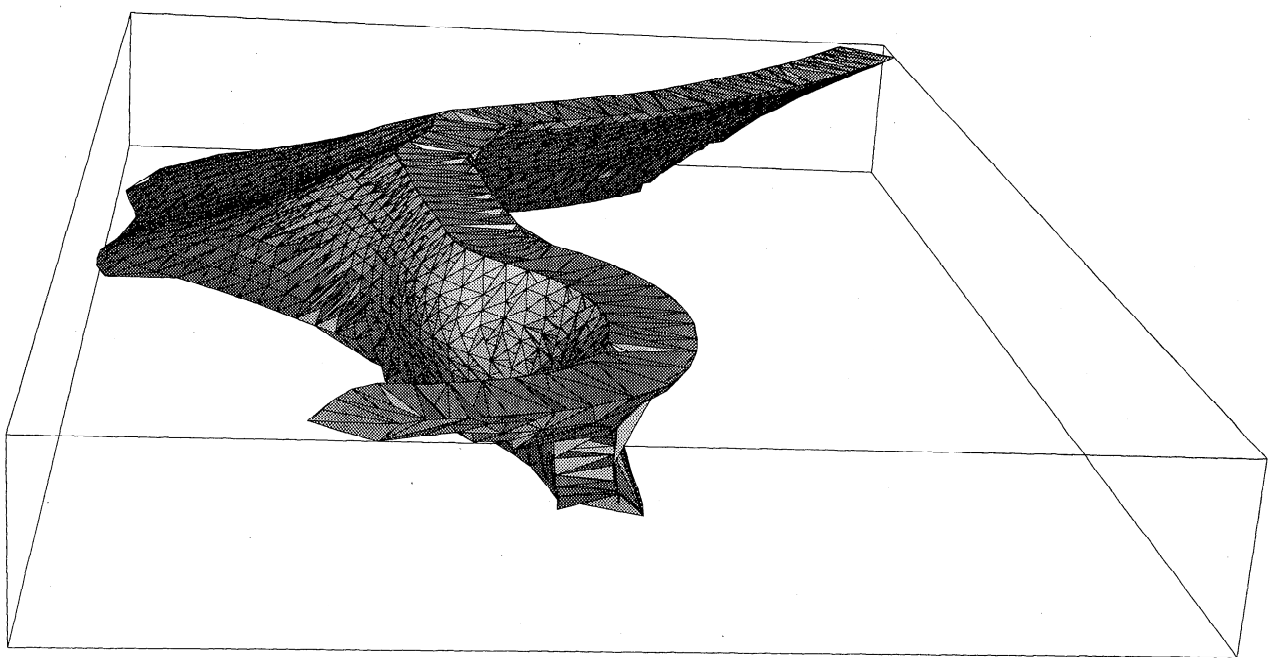

Figure 2c. A perspective view of the slabs of the northwest Pacific from above and the southwest. The edges of individual Delaunay tetrahedra are shown in black.

3.3. Summary of Parameterization

In summary, the parameterization of the upper mantle consists of two distinct elements: Delaunay tetrahedra to define slabs and a two-dimensional grid of Voronoi cells extended uniformly to a depth of 660 km to define tectonic regions. The slabs are overlaid on the regionalization. To determine which type of environment a given point (along a ray) is in, we first detect if it is within a slab. If it is not, its position in the regionalization is determined. Thus we represent complex structures efficiently and economic algorithms are available to locate any arbitrary point in either irregular grid [see *Sambridge and Gudmundsson,* 1998]. The parameterization includes fine spatial features in subduction zones on a scale of 10 km and also tectonic age provinces a few thousand kilometers across. Its dynamic range is thus 2-3 orders of magnitude.

3.4. Data Selection

Researchers who use the ISC database of travel time picks often emphasize the importance of the large number of data it contains. Their argument is that the data contain errors that due to their randomness are suppressed when averaging a large number of observations. We question the assumption of randomness. In particular, it is likely that earthquakes are systematically mislocated on scales correlating with tectonic features. Therefore we use a select data set of travel times from well-located events and nuclear explosions in order to alleviate the mapping of mislocation into structure. This is of particular importance in building a reference Earth model because observed biases in earthquake location can be significant and can inject artificial structural signal into travel times of the order of seconds. The events we use are the 105 events of the test data set used by *Kennett and Engdahl* [1991] supplemented with 92 large earthquakes to get a more even sampling of the globe and the nine tectonic regions. The criterion for the selection of these events was that they be recorded by a large number of globally distributed stations. Their locations are taken from nuclear agencies, from local and regional networks, and if neither of the above is available, from the relocated catalog of Engdahl et al. (submitted manuscript, 1997). They reassociated ISC data, included pP and pwP phases in the location, used IASP91 [*Kennett and Engdahl,* 1991], and subjected locations to stringent fitness criteria. We use only teleseismic P and $PKIKP$ arrivals (first arrivals) for the compressional velocity model and teleseismic S arrivals for the shear velocity structure. We use only picks reported to the ISC as impulsive to insure a high degree of robustness of individual picks.

All the data have been corrected for the Earth's ellipticity [*Kennett and Gudmundsson,* 1996], for station elevation, and for surface topography/bathymetry in the case of phases reflecting off the Earth's surface. We have prepared data from other phases such as pP, PP, PcP, PKP, sS, SS, ScS, and SKS from the 197 events in this select data set.

Figure 3 shows a map of the 197 events used together with the regionalization. The events are grouped into three categories. First, there are 21 nuclear and chemical explosions (displayed as stars in Figure 3). Their locations will be taken to be fixed. Second, there are 39 earthquakes which are well located with local obser-

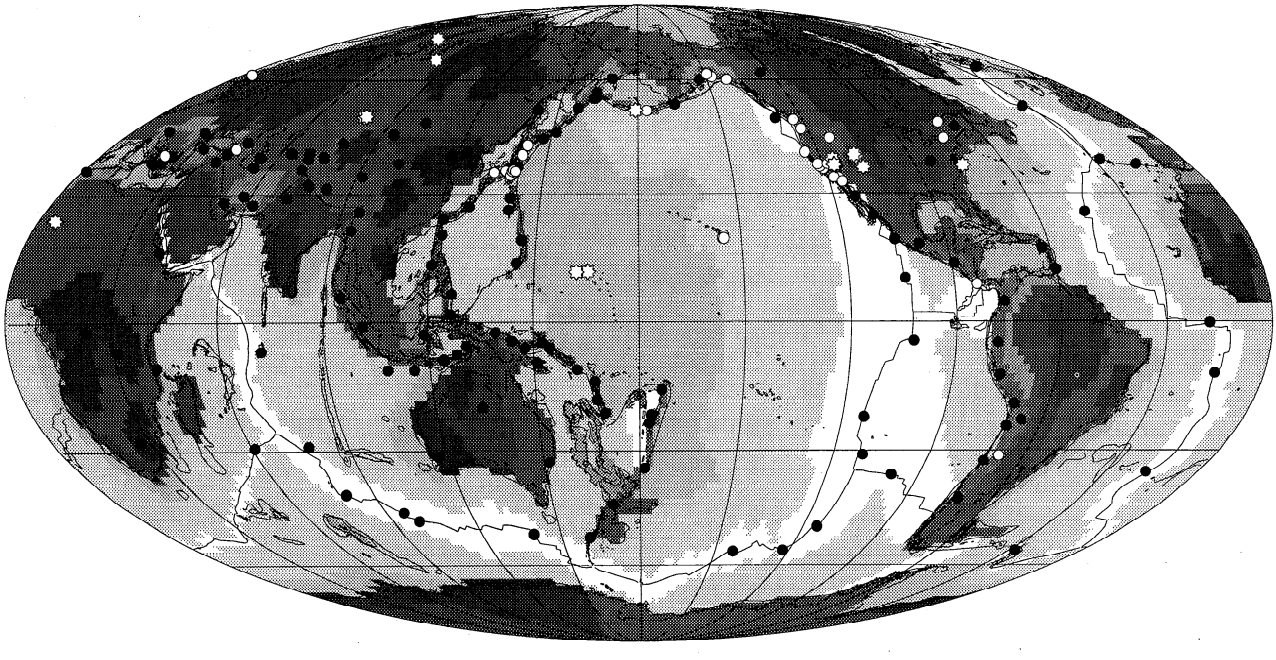

Figure 3. Epicenters of the 197 events used in this study with regionalization for reference. Stars represent artificial explosions, open dots represent events located within a regional network of stations, and solid dots represent events located using global observations.

vations in a local velocity model. They are displayed as open dots. Their locations are also assumed fixed. Then, the remaining 137 events (shown as solid dots) are located using teleseismic observations and are allowed to vary in their origin time and depth.

We reference travel time residuals to the AK135 model [*Kennett et al.*, 1995] and reassociate all impulsive picks reported to the ISC for the above events. We find a surprising number of events with a significant mean residual. This is surprising because AK135 is almost identical in the mantle to IASP91 which Engdahl et al. (submitted manuscript, 1997) used for their locations. The explanation must lie in a difference in data selection. We, for example, include *PKIKP* and not *pP*. We do not associate *pwP*. The large number of events with a significant apparent origin time shift led us to allow origin time to be a free parameter in our inversion for regionalized structure. Allowing origin time to vary independently for P and S is equivalent to allowing for a relocation in source depth and origin time. We find 14,291 P and *PKIKP* picks and 2608 S picks which satisfy our selection criteria.

4. Inversion: Data Reduction

We solve a linearized inverse problem. A higher-order approach is not warranted because ray bending critically depends on velocity gradients which are artificially represented by our parameterization. We sample depth 10 times at 66 km spacing and seek nine independent velocity profiles, one for each of the eight tectonic regions as well as slabs. We use a standard damped-least-squares inversion procedure. In regions with limited depth distribution of sources, teleseismic rays give limited depth resolution in the upper mantle. We cannot well resolve 10 independent parameters except in subducting slabs, where there is a distribution of events in depth. Since the level of heterogeneity in the upper mantle is strongly concentrated near the surface [e.g., *Gudmundsson et al.*, 1990], in the top 300-400 km, we have projected the depth profiles on to a set of four Gaussian basis functions which are not allowed to put structure in the lower half of the upper mantle. In effect, we are implementing depth-dependent damping. We argue that this is in line with our general approach of applying stringent geometrical constraints to the inversion based on a priori information. The basis functions are not orthogonal in themselves but decompose into a fourfold orthogonal basis. The model for subducted lithosphere is allowed to vary throughout the upper mantle. The results we present are moderately damped. The trade-off employed to select the damping was that of variance reduction versus damping coefficient (which varies monotonically with resolution). The damping was selected where it started to significantly affect the variance reduction (lowered by 10–20%). The relocation component of the inverse problem is scaled to allow for virtually full removal of average residuals for each event.

For the P wave data, origin time shifts of 137 events out of 192 account for about 55% variance reduction (see Table 1). An undamped inversion allowing for 10 independent depth parameters in each region achieves a 19% variance reduction. Limiting the degrees of freedom to four per region via the Gaussian basis reduces the variance reduction to 16%. We have damped the solution to yield a variance reduction of 14%. For the S wave data the pattern is similar, with the damped model achieving a 10% variance reduction. For the S waves the variance is considerably higher than for the P waves, and the relative variance reduction achieved by origin time shift is much less than for the P wave data.

We find that none of the minor data sets consisting of the compressional *pP*, *PP*, *PcP*, and *PKP* phases or the shear *sS*, *SS*, *ScS*, and *SKS* phases improve resolution significantly nor are they consistent with the major data sets of *P*, *PKIKP*, or *S* phases. The RUM model does not significantly reduce the variance of the minor data sets. These minor phases are all secondary, and their travel times are thus less precisely read from a seismogram than for the primary phases. Furthermore, their frequency of observation is much less than that of the primary phases. We can only suggest that the structural signal in those minor phases is swamped by their observational errors.

As a final step in the data reduction, we estimate station corrections to be applied after correction for the RUM model. We evaluate a correction only for stations with more than four picks reported. The station correction is simply the average residual for each station after correction for the RUM model. This step achieves a further variance reduction of 16% and 11% for the P waves and S waves, respectively. Table 1 summarizes the reduction of the mean and variance of the P and S wave data by the individual steps of the data reduction. Figure 4 shows a histogram of time residuals before and after data reduction. We note that the quoted variance reduction applies to individual picks, not to summary rays. We also note that the remaining variance in the data is comparable to, but slightly higher than, the esti-

Table 1. Mean and Variance Reduction After the Different Steps of Inversion/Data Reduction

	Mean s	Variance s^2	Variance Reduction percent
P Residuals			
Initial P residuals	1.18	4.30	
After relocation	0.69	1.99	54
After velocity perturbation	0.19	1.71	14
After station correction	0.04	1.44	16
S Residuals			
Initial S residuals	0.51	35.8	
After relocation	-0.17	30.0	16
After velocity perturbation	0.01	26.9	10
After station corrections	-0.03	23.9	11

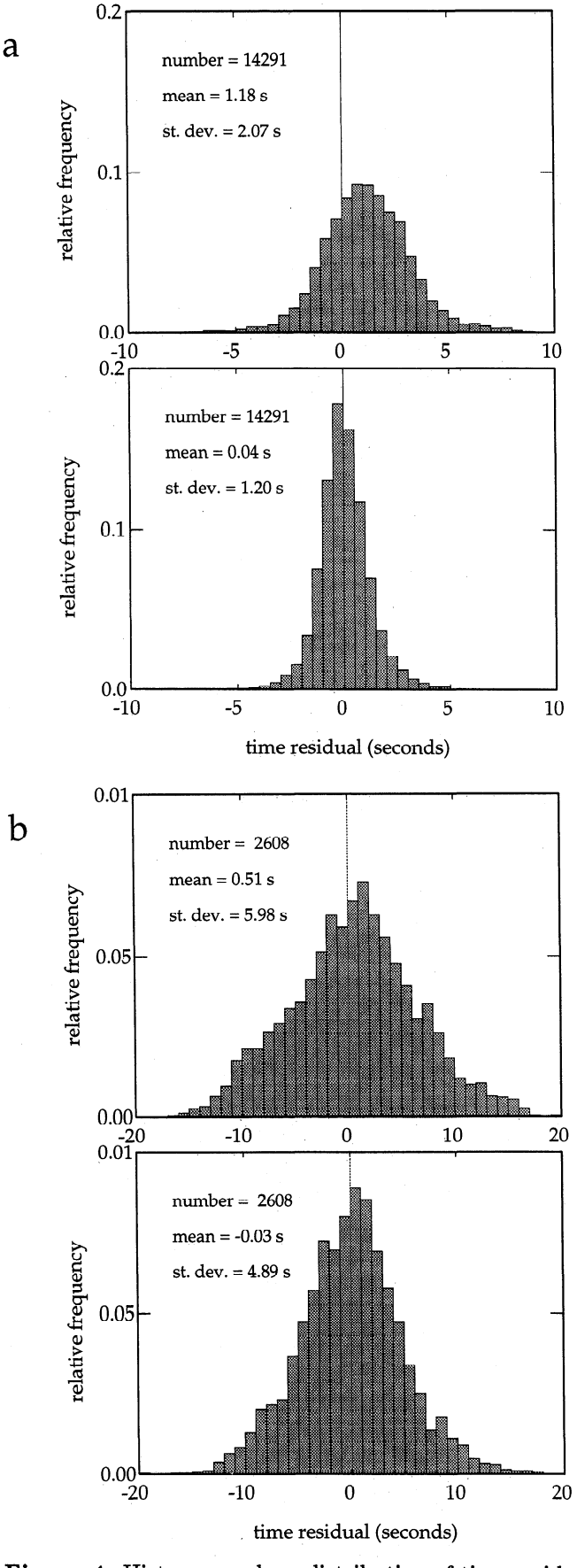

Figure 4. Histograms show distribution of time residuals before and after inversion/data reduction. (a) P wave residuals. (b) S wave residuals.

mates of noise variance in the ISC data for teleseismic P and S waves by *Gudmundsson et al.* [1990] and *Davies et al.* [1992].

5. Results

The results of the inversion are shown in Figure 5 and Table 2. In Figure 5 each function of depth represents a velocity perturbation for a given tectonic region. Figure 5a shows the results for P waves, and Figure 5b shows the results for S waves. The results are plotted as a relative velocity perturbation (in percent) with one standard deviation error bars assuming that the error variance is as given by *Gudmundsson et al.* [1990] for the teleseismic P wave data, i.e., $1s^2$, and by *Davies et al.* [1992] for teleseismic S wave data, i.e., $8s^2$. Table 2 also list the results as relative velocity perturbations.

The results for compressional velocity are encouraging. Slabs appear as a continuous fast anomaly throughout the upper mantle except at the top where we have tectonic crust rather than a true slab and where the result is probably affected by the slow mantle wedge. The amplitude of the slab structure is 2-3% velocity perturbation. This is assumed to be uniform over a thickness of 200 km. The subducting lithosphere is probably not that thick at shallow depths, but the associated thermal anomaly diffuses with time or depth. Furthermore, it would peak above its average level. The 2-3% level of perturbation in the slabs would thus be consistent with a somewhat higher peak perturbation in the core of the slabs, possibly as high as 5%. This is a reasonable level of perturbation compared to predictions on the basis of thermal modeling. Other features of the results are also encouraging. The oceans are slow with old oceans developing a fast lithosphere. Tectonic continent and young continent are also slow and essentially indistinguishable. This is of interest because, e.g., *Nataf and Ricard* [1996] do not make a distinction between those regions in their regionalization. That decision appears to have been justified. Currently active continental margins and island arcs are not clearly distinguishable from other Mesozoic continental regions. Intermediate-age continents have developed a fast lithosphere, while their asthenosphere looks much like that of young continental regions. There is no resolvable structure underneath old continents, suggesting that AK135 (and IASP91) is representative of continents in that age range. This is interesting and not surprising because the AK135 and IASP91 models were not designed to represent average Earth structure but rather as effective reference models for travel time prediction deliberately biased according to the distribution of stations. Ancient continents are fast, but not to a great depth, only about 200 km. Note, however, that depth resolution is limited. It should be noted that we have not corrected for crustal structure so the model should be interpreted to include crustal signature. The number of degrees of freedom in the compressional model is 22 (trace of resolution matrix).

The RUM model compares remarkably well with the 3SMAC model of *Nataf and Ricard* [1996]. Compar-

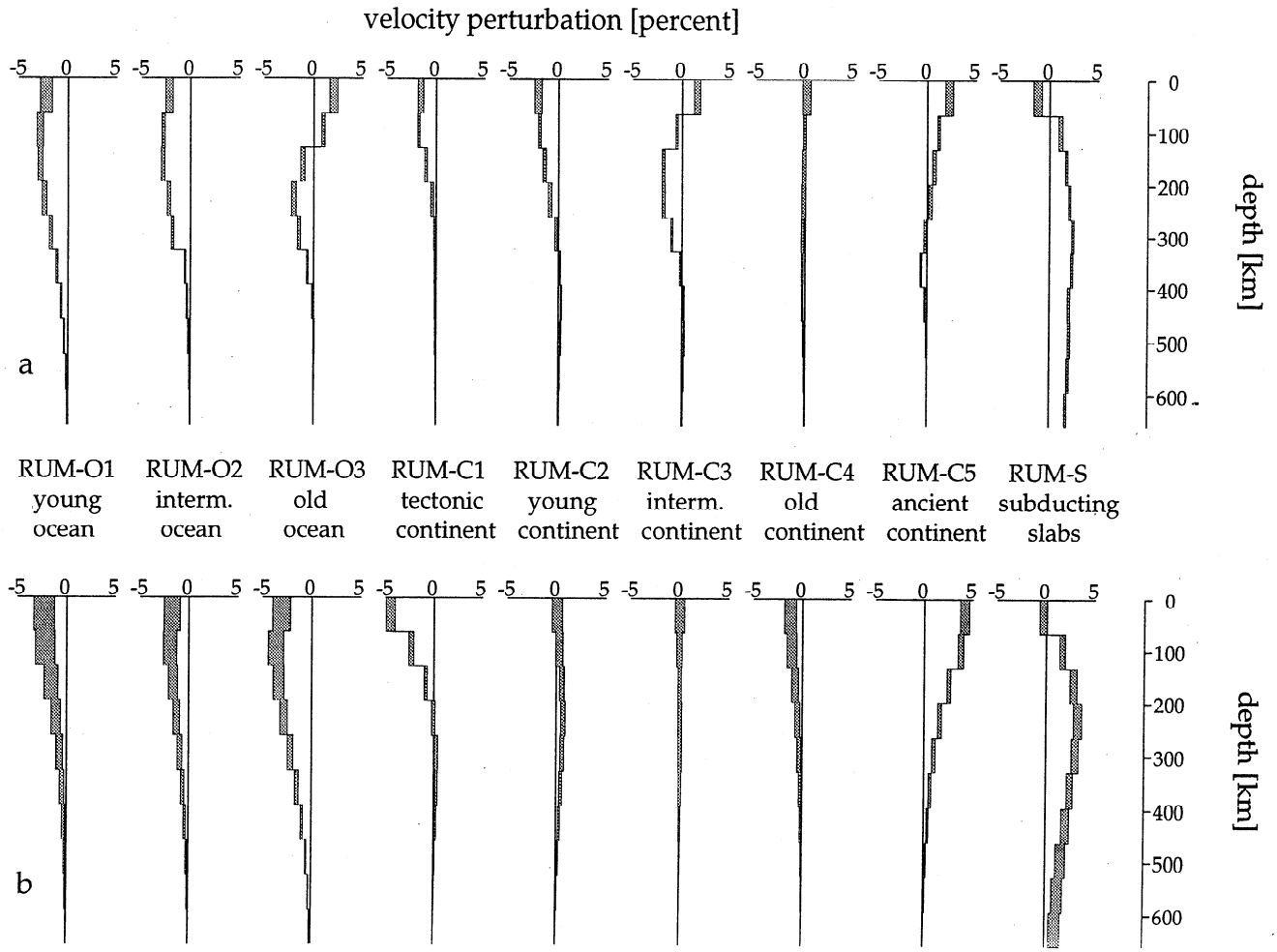

Figure 5. The RUM velocity model presented as percentile velocity perturbation from AK135 model. (a) For compressional velocity. (b) For shear velocity. The shaded area represents the range $\pm\sigma$, where σ is one standard deviation.

ing Figure 5 with their Figures 12 and 13 reveals that subducting slabs represent a similar level of perturbation from the IASP91 model as RUM does from the AK135 model. The same holds in a general sense for oceans, tectonic areas and shields. Note, however, that the level of perturbation in the RUM-C5 (ancient continent) model is less than the 3SMAC prediction for the Canadian shield. This discrepancy is rectified by the station corrections on the Canadian shield which according to RUM has a higher-velocity substructure than the average shield.

The RUM model is best compared to individual one-dimensional models by comparing the integral travel time anomaly at vertical incidence. The RUM model gives a range from -0.25 to 1.16 s relative to AK135. The negative (fast) extreme corresponds to ancient continent while the positive (slow) extreme corresponds to young ocean. Shield models, such as S25 of *Lefevre and Helmberger* [1989] for the Laurentian shield, QUARTZN of *Mechie et al.* [1993] for the Fennorussian shield, and FLSB of *Kennett et al.* [1994] for the Australian shield, have an average travel time anomaly of about -1 s. The tectonic models T7 and T9 of *Burdick and Helmberger* [1978] and *Burdick* [1981] average at about 0.6 s. Tectonic continent in RUM has an anomaly of about 0.5 s. The oceanic models GCA and CJF of *Walck* [1984, 1985] average at 0.2 s. The range is the same for the elements of RUM and the one-dimensional models, i.e., about 1.5 s. The time anomaly for tectonic continent is similar in RUM as in tectonic one-dimensional models, but for shield models and oceanic models there is a shift of about 1 s. We suggest a few potential explanations of this discrepancy. Stations and events are colocated in tectonic regions. Therefore one-dimensional refraction type studies enjoy good constraints on shallow structure. This is not the case in shield regions or oceanic regions. The stations are removed from the seismicity. Therefore the shallow constraint is poor and/or the paths tectonically mixed at short distance. From Figure 3 it is evident that we do not have any events in young oceanic regions that are constrained by local observations. Neither do we have such events in shield regions. The RUM model may therefore suffer from a lack of absolute reference in those regions. On the other hand, stations in shield regions record many of the locally constrained events which adds absolute constraint

Table 2. RUM Model as a Percentile Slowness Perturbation Relative to AK135

Depth, km	RUM O1	RUM O2	RUM O3	RUM C1	RUM C2	RUM C3	RUM C4	RUM C5	RUM S
				Compressional Velocity					
33	2.23	2.19	-2.03	2.08	1.58	-1.53	-0.14	-2.24	1.23
99	2.84	2.78	-0.96	1.94	1.77	0.54	0.07	-1.16	-1.12
165	2.81	2.84	1.14	1.45	1.04	1.91	0.13	-0.71	-1.73
231	2.41	2.23	2.04	0.89	0.42	1.90	0.17	-0.31	-2.06
297	1.76	1.84	1.52	0.27	0.17	1.05	0.26	0.25	-2.38
363	1.13	0.56	0.65	-0.13	0.11	0.20	0.29	0.65	-2.29
429	0.68	0.37	0.13	-0.27	0.09	-0.20	0.26	0.26	-2.00
495	0.38	0.22	-0.04	-0.23	0.06	-0.24	0.18	0.09	-2.01
561	0.20	0.12	-0.05	-0.14	0.04	-0.16	0.10	0.03	-1.89
627	0.10	0.06	-0.03	-0.07	0.02	-0.09	0.05	0.01	-1.70
				Shear Velocity					
33	2.29	1.73	3.08	-0.08	4.46	-0.00	1.24	-4.15	0.29
99	2.18	1.93	3.65	-0.29	2.32	0.04	1.09	-3.75	-1.68
165	1.58	1.61	3.36	-0.57	0.82	-0.00	0.75	-2.55	-2.79
231	1.07	1.25	2.84	-0.68	0.03	-0.03	0.50	-1.61	-3.25
297	0.71	0.91	2.17	-0.60	-0.25	-0.04	0.32	-1.00	-2.96
363	0.46	0.62	1.51	-0.45	-0.26	-0.03	0.21	-0.63	-2.44
429	0.30	0.40	0.99	-0.30	-0.18	-0.02	0.13	-0.40	-2.00
495	0.17	0.24	0.58	-0.18	-0.11	-0.01	0.08	-0.23	-1.54
561	0.09	0.13	0.32	-0.10	-0.06	-0.01	0.04	-0.13	-1.23
627	0.05	0.06	0.16	-0.05	-0.03	-0.00	0.02	-0.06	-0.98

The labeling of the regions is as in Figure 5.

to the shields. The RUM model represents an average property for all regions of the same tectonic type. Station corrections (discussed below) indicate that considerable variability exists among regions of the same type. It is possible that published one-dimensional, regional models are not representative of their regions.

The results for the shear velocity are less well constrained and more poorly resolved. This is because of fewer and poorer data. In order to render the result interpretable in the sense of suppressing noise sufficiently so that model exceeds uncertainty in amplitude, we have had to damp the S wave model more heavily than the P wave model. The number of degrees of freedom in the shear velocity model is only 11. Still subducted lithosphere extends as a fast anomaly of reasonable amplitude throughout the upper mantle; old continental cores are fast and oceans are slow. The absence of a lithosphere in the oceans may be ascribed to lower resolution. The reduced level of coherency in the transition from young ocean to ancient continent can be understood in terms of poorer constraint. The range of the predicted vertical travel time anomaly for RUM-S (S wave model) is -2.1 s for ancient continents, which is comparable to the SNA model of *Grand and Helmberger* [1984] and the NJPB model of *Kennett et al.* [1994] for the North American and Australian shields, respectively, to about 2 s in the oceans. The vertical time delay for the tectonic regions of RUM-S is only about 1 s, while the *tna* model of *Grand and Helmberger* [1984] has a 7.5 s delay. Here the agreement in the tectonic region is of the same sense but poor in amplitude.

We refrain from interpreting the results beyond pointing out that despite strict geometrical constraints on the lateral extent of anomalies the level of velocity perturbation is reasonable. Any comparison between the results for P waves and S waves would have to take into account the difference in the damping of the two models. The S wave model is more heavily damped than the P wave model, which qualitatively explains why the modeled perturbation in shear velocity does not clearly exceed the perturbation of compressional velocity (we would expect the former to exceed the latter by $50 - 100\%$). Surface waves may be better suited to study the shear velocity heterogeneity of the upper mantle than delay times.

Our confidence in the results is much higher for compressional velocity than shear velocity. It is interesting to display the model in its full three dimensionality. Figure 6 shows a pair of cross sections through the RUM-P model (P wave model). In Figure 6a the section cuts through the Tongan slab, the Banda Sea slab near its sharp bend, some shallow slabs in the Philippines, and the Andean slab. It also grazes through the Hellenic slab. In Figure 6b the cross section cuts through the Su-

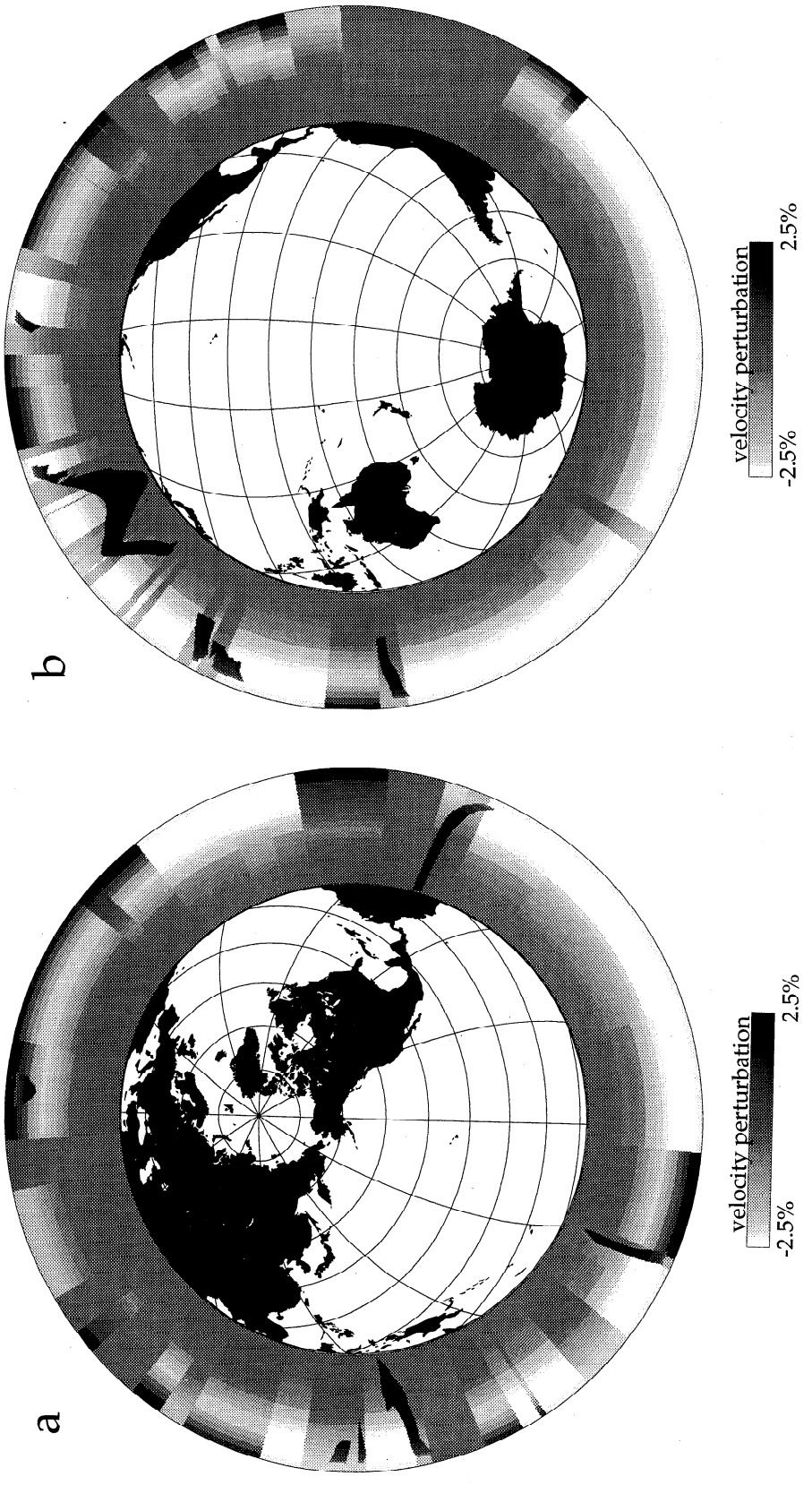

Figure 6. Two cross sections through the three-dimensional RUM model showing the range of velocity perturbations and demonstrating the types of bodies included in the model. (a) With normal at N56.67° latitude and W150° longitude. (b) With normal at S17.85° latitude and W30° longitude. Note that this global model contains clear slabs in the upper mantle.

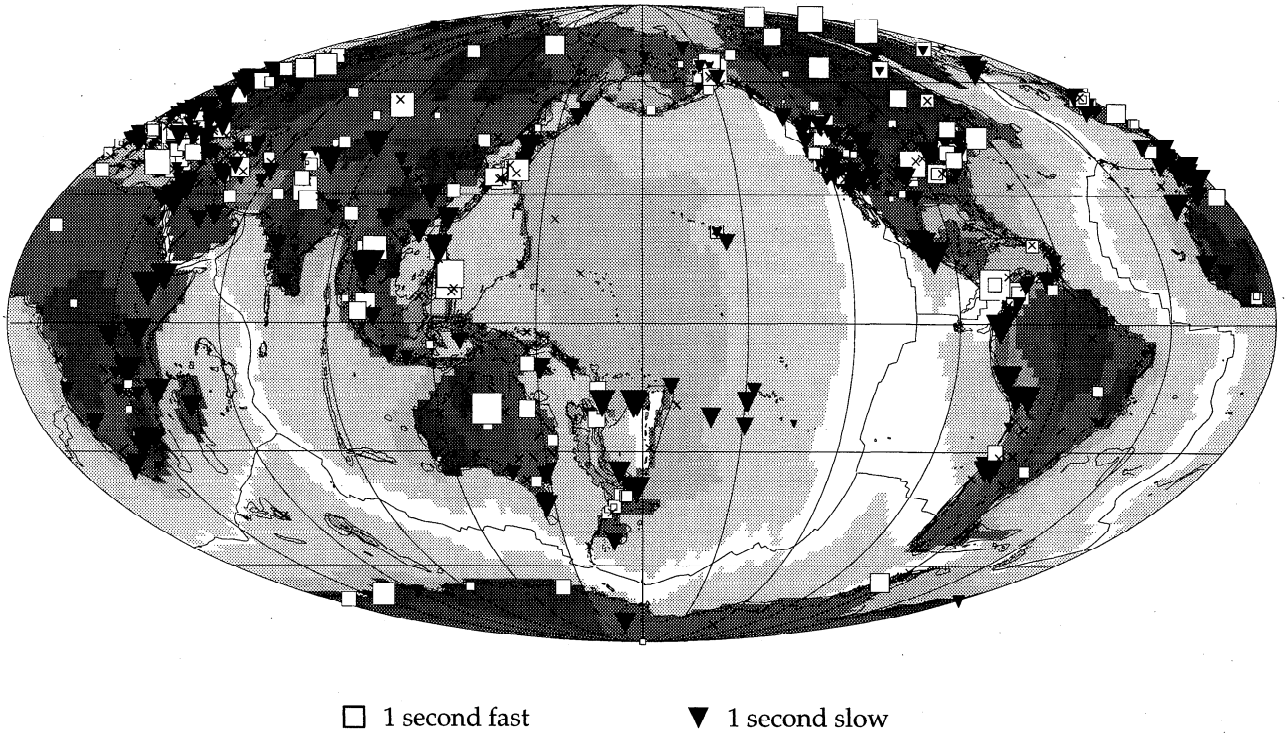

Figure 7. Station corrections for P wave residuals after correction for the RUM model. Squares represent negative corrections (fast); triangles represent positive corrections (slow). The symbol area is proportional to the amplitude of the correction with 1 s corrections given in legend for reference.

materan slab, shallow slabs in the Philippines, and the slabs of the northwestern Pacific along strike. Subducting lithosphere constitutes a major feature of the RUM model at the extremity of fast perturbations. Their geometry is imposed. This may render the estimate of their overall velocity perturbation more robust than in less constrained delay time models of slab regions. The velocity perturbations in the upper mantle range between ±2.5%, which is similar to what one might expect on the basis of estimates of $\nu = \partial \ln Vs / \partial \ln Vp$ and the heterogeneity pattern as modeled from surface wave data.

Figure 7 shows the station corrections for P wave residuals. A corresponding map for S wave residuals is not presented because of its sparseness and how poorly constrained we regard the shear velocity model. Clearly, a significant signal is left in the data after inversion for regionalized structure. Note, for example, that a fast anomaly remains within the Laurentian craton. On the other hand, the African cratons are left with slow anomalies. This is in agreement with results of global, surface wave tomography which has the African cratons show up much less clearly than, e.g., the Laurentian, Fennorussian, and Australian cratons. Some tectonic regions are left with systematically fast residuals, while others are slow. Considerable scatter is evident within some regions. Clearly, all regions of the same type are not the same. Furthermore, small-scale structure within individual regions is not modeled but instead is absorbed in station corrections.

6. Locating Known Events

To test the success of the RUM model as a reference for teleseismic travel times, we relocate 19 of the 21 explosions in the data set. The locations of those 19 explosions can be regarded as known [*Kennett and Engdahl,* 1991]. We compare relocations using teleseismic P residuals which are referenced to the AK135 model, to the RUM-P model, and to the RUM-P model as well as station corrections. We relocate only the epicenter, i.e., the depth is fixed at the reported depth. Many of the earlier events in particular have a very unevenly distributed sampling. The locations become much more robust by evening this distribution or declustering it. For each event we construct a kernel matrix which is nx3, where n is the number of observations. The three elements of each row are the sensitivity to relocation in latitude, longitude, and origin time (the last is always -1). We bin the first and second columns of the kernel matrix four times each. After removing outliers (residuals more than 5 s away from mean of bin) we calculate an average residual for each of the 16 bins downweighting emergent picks. This procedure has a similar effect in improving the robustness of location to the weighting scheme employed by *Smith and Ekström* [1996]. We use only P residuals in the teleseismic range. Finally, we solve a linearized relocation problem giving all bins equal weight. In effect, we are declustering the sampling of the focal sphere as seen from the event to minimize biases in the relocation. The procedure of the relocation

Table 3. Mislocation of Explosions of Known Location After Correction for the RUM Model and the Associated Station Corrections

	AK135		AK135 + RUM		AK135 + RUM + Station corr.	
	σ_t, s	σ_h, km	σ_t, s	σ_h, km	σ_t, s	σ_h, km
Castle Bravo	-0.13	14.03	0.48	11.85	0.40	10.85
Castle Yankee	-0.22	9.43	0.42	6.84	0.36	5.28
Oak	-0.10	8.27	0.45	6.04	0.46	4.71
Bilby	-0.18	6.20	0.78	5.54	0.75	5.93
Sahara Oct. 20 1963	-0.07	8.72	0.35	9.19	0.73	5.89
Sahara Feb. 27 1965	-0.27	11.09	0.10	10.61	0.61	5.12
Chase	-1.11	8.41	-0.46	4.29	-0.39	1.55
Commodore	-0.90	16.18	0.16	9.39	0.34	4.75
Gasbuggy	-0.81	2.79	-0.56	1.67	-0.54	4.06
Faultless	-0.58	9.48	0.46	3.33	0.59	6.03
Boxcar	-0.49	8.46	0.52	2.75	0.65	4.84
Rulison	-0.86	13.32	-0.53	15.19	-0.24	6.22
Kazakh Nov. 30 1969	0.78	7.59	1.14	8.10	1.04	2.39
Kazakh Apr. 25 1971	0.55	10.72	0.90	11.18	0.80	5.53
Cannikin	1.55	22.32	1.88	14.28	1.90	11.60
Kazakh Aug. 16 1972	0.85	11.79	1.21	12.06	0.89	4.72
Kazakh Nov. 02 1972	0.79	9.71	1.11	9.49	1.25	3.86
Rio Blanco	-0.60	9.24	-0.26	11.19	-0.31	8.80
Alamo	-0.59	11.73	0.34	5.33	0.38	6.21
RMS	0.71	11.23	0.77	9.16	0.77	6.19

Only teleseismic residuals were used.

is the same for all events and for all levels of data reduction. The results of the relocations are listed in Table 3 as misfit in origin time (seconds) and length of the horizontal mislocation vector (kilometers) and summarized at the bottom as the root-mean-square (rms) misfit in time and horizontally. The mislocations of individual events using AK135 for reference are similar to the mislocations reported by *Kennett and Engdahl* [1991]. In other words, the level of robustness of the location procedure is similar although the procedures differ. After correction of residuals for the RUM three-dimensional model the mislocations are significantly improved, i.e., by about 20%. Applying the RUM station corrections reduces the rms misfit by a further 33%. While it is tempting to compare the rms misfit to that achieved by *Smith and Ekström* [1996], in absolute terms that would have limited meaning because the location procedure is not the same.

A significant level of reduction of mislocation is related to the application of station corrections. The RUM model's usefulness for travel time corrections lies in the fact that the corrections are derived from a model and that it effectively implements corrections for near-source structure, event corrections. Where a station's history does not allow for a robust station correction, the model provides a reasonable means of predicting that station correction to first order.

7. Conclusions

We have described upper mantle structure with 22 degrees of freedom (compressional velocity) and 11 degrees of freedom (shear velocity) and managed to explain a significant portion of the apparent structural variance in travel time data. The data are individual, not summary ray data. S wave residuals give results similar to the P wave velocity variations but less well constrained. Our parameterization, in effect, imposes complex spatial constraints on this inversion for upper mantle structure which we can think of as a priori information, i.e., the presumption that the upper mantle can be regionalized as we have done. The success of the inversion justifies those constraints. The remaining station residuals point to the fact that this regionalized description is not complete, however, and that on order of half the structural signal in the data is explained by it. The RUM model is derived as a regionalized reference model for the upper mantle. It should prove useful for correcting travel times for upper mantle heterogeneity to first order. Improvements in the location misfit of known explosions demonstrates the model's success. The RUM model can be used as an initial reference model for tomography. It should also prove useful to provide a first-order estimate of structure in regions of sparse data coverage.

The RUM model is tabulated in Table 2. We have also prepared a home page on the World-Wide Web at http://rses.anu.edu.au/RUM/rum.html with graphical information, software, and software description. The software includes codes to calculate travel time corrections for the RUM model for a variety of phases including other first-order effects such as due to the Earth's topography.

Acknowledgments. We are indebted to Ken Creager for many useful discussions about slab morphology and for teaching us to use his interactive contouring routines for MATLAB. Henry-Claude Nataf and Peter Shearer provided constructive criticism. We acknowledge useful discussions with Brian Kennett. This work was supported in part by a grant from the U.S. Air Force Office of Scientific Research F49620-94-1-0022, F49620-94-1-0110.

References

Bott, M.H.P., and K. Gunnarsson, Crustal structure of the Iceland-Faeroe Ridge, *J. Geophys., 47,* 221-227, 1980.

Burdick, L.J., A comparison of the upper-mantle structure beneath North America and Europe, *J. Geophys. Res., 86,* 5926-5936, 1981.

Burdick, L.J., and D.V. Helmberger, The upper mantle *P* velocity structure of the western United States, *J. Geophys. Res., 83,* 1699-1712, 1978.

Davies, J.H., Ó. Gudmundsson, and R.W. Clayton, Spectra of mantle shear velocity structure, *Geophys. J. Int., 108,* 865-882, 1992.

Debayle, E., and J.J. Leveque, Upper mantle heterogeneities in the Indian Ocean from waveform inversion, *Geophys. Res. Lett., , 24,* 245-248, 1997.

Fujita, K., E.R. Engdahl, and N.H. Sleep, Subduction-zone calibration and teleseismic relocation of thrust-zone events in the central Aleutian Islands, *Bull. Seismol. Soc. Am., 71,* 1805-1828, 1981.

Grand, S., and D.V. Helmberger, Upper-mantle shear structure of North America, *Geophys. J. R. Astron. Soc., 76,* 399-438, 1984.

Gudmundsson, Ó., J.H. Davies, and R.W. Clayton, Stochastic analysis of global travel time data: Mantle heterogeneity and errors in the ISC data, *Geophys. J. Int., 102,* 25-43, 1990.

Helmberger, D.V., and R.A. Wiggins, Upper mantle structure of the midwestern United States, *J. Geophys. Res., 76,* 3229-3245, 1971.

Jordan, T., Global tectonic regionalisation for seismological data analysis, *Bull. Seismol. Soc. Am., 71,* 1131-1141, 1981.

Kennett, B.L.N., and E.R. Engdahl, Traveltimes for global earthquake location and phase identification, *Geophys. J. Int., 105,* 429-465, 1991.

Kennett, B.L.N., and Ó. Gudmundsson, Ellipticity corrections for seismic phases, *Geophys. J. Int., 127,* 40-48, 1996.

Kennett, B.L.N., Ó. Gudmundsson, and C. Tong, The upper mantle S and P velocity structure beneath northern Australia from broad-band observations, *Phys. Earth Planet. Inter., 86,* 85-98, 1994.

Kennett, B.L.N., E.R. Engdahl, and R. Buland, Travel times for global earthquake location and phase association, *Geophys. J. Int., 122,* 108-124, 1995.

Lefevre, L.V., and D.V. Helmberger, Upper mantle *P* velocity structure of the Canadian shield, *J. Geophys. Res., 94,* 17,749-17,765, 1989.

Mechie, J., A.V. Egorkin, K. Fuchs, T. Ryberg, L. Solodilov, and F. Wenzel, P-wave mantle velocity structure beneath northern Eurasia from long range recordings along the profile quartz, *Phys. Earth Planet. Inter., 79,* 269-286, 1993.

Montagner, J.-P., and T. Tanimoto, Global upper mantle tomography of seismic velocities and anisotropies, *J. Geophys. Res., 96,* 20,337-20,351, 1991.

Nataf, H.-C., and Y. Ricard, 3SMAC: An a priori tomographic model of the upper mantle based on geophysical modeling, *Phys. Earth Planet. Inter., 95,* 101-122, 1996.

Nolet, G., S.P. Grand, and B.L.N. Kennett, Seismic heterogeneity in the upper mantle, *J. Geophys. Res., 99,*-23,753-23,766, 1994.

Okabe, A., B. Boots, and K. Sugihara, *Spatial-Tesselation Concepts and Applications of Voronoi Diagrams,* John Wiley, New York, 1992.

Ricard, Y., H.-C. Nataf, and J.-P. Montagner, The tree-dimensional seismological model a priori constrained: Confrontation with seismic data, *J. Geophys. Res., 101,* 8457-8472, 1996.

Romanowicz, B., Seismic tomography of the Earth's mantle, *Annu. Rev. Earth Planet. Sci., 19,* 77-99, 1991.

Sambridge, M., and Ó. Gudmundsson, Tomographic systems of equations with irregular cells, *J. Geophys. Res., in press,* 1998.

Sambridge, M., J. Braun, and H. McQueen, Geophysical parameterisation and interpolation of irregular data using natural neighbours, *Geophys. J. Int., 122,* 837-857, 1995.

Sclater J.G., C. Jaupart, and D. Galson, The heat flow through oceanic and continental crust and the heat loss of the Earth, *Rev. Geophys., 18,* 269-311, 1980.

Smith, G.P., and G. Ekström, Improving teleseismic event locations using a three-dimensional Earth model, *Bull. Seismol. Soc. Am., 86,* 788-796, 1996.

Spakman, W., M.J.R. Wortel, and N.J. Vlaar, The Hellenic subduction zone: A tomographic image and its geodynamic implications, *Geophys. Res. Lett., 15,* 60-63, 1988.

Trampert, J., and J.H. Woodhouse, Global phase velocity maps of Love and Rayleigh waves between 40 and 150 seconds, *Geophys. J. Int., 122,* 675-690, 1995.

van der Hilst, R., R. Engdahl, W. Spakman, and G. Nolet, Tomographic imaging of subducted lithosphere below northwest Pacific island arcs, *Nature, 353,* 37-43, 1991.

van der Hilst, R., E.R. Engdahl, and W. Spakman, Tomographic inversion of P and pP data for aspherical structure below the northwest Pacific region, *Geophys. J. Int., 115,* 264-302, 1993.

Walck, M.C., The P-wave upper mantle structure beneath an active spreading center: The Gulf of California, *Geophys. J. R. Astron. Soc., 76,* 697-723, 1984.

Walck, M.C., The upper mantle beneath the north-east Pacific rim: A comparison with the Gulf of California, *Geophys. J. R. Astron. Soc., 81,* 243-276, 1985.

Widiyantoro, S., and R. van der Hilst, Structure and evolution of lithospheric slab beneath the Sunda arc, Indonesia, *Science, 271,* 1566-1570, 1996.

Woodhouse, J.H., and A. Dziewonski, Mapping the upper mantle: Three-dimensional modeling of Earth structure by inversion of seismic waveforms, *J. Geophys. Res., 89,* 5953-5986, 1984.

Woodhouse, J.H., and J. Trampert, New geodynamical constraints from seismic tomography, *Earth Planet. Sci. Lett., in press,* 1997.

Zhang, Y.-S., and T. Lay, Global surface wave phase velocity variations, *J. Geophys. Res., 101,* 8415-8436, 1996.

Zhang, Y.-S., and T. Tanimoto, High-resolution global upper mantle structure and plate tectonics, *J. Geophys. Res., 98,* 9793-9823, 1993.

Zhao, D.-P., A. Hasegawa, and S. Horiuchi, Tomographic imaging of *P* and *S* wave velocity structure beneath northeastern Japan, *J. Geophys. Res., 97,* 19,909-19,928, 1992.

Zhou, H.-W., and R.W. Clayton, *P* and *S* travel time inversions for subducting slab under the island arcs of the northwest Pacific, *J. Geophys. Res., 95,* 6829-6851, 1990.

Zielhuis, A., and G. Nolet, Shear-wave velocity variations in the upper mantle beneath central Europe, *Geophys. J. Int., 117,* 695-715, 1994.

Ó. Gudmundsson and M. Sambridge, Research School of Earth Sciences, The Australian National University, Canberra, ACT 0200, Australia. (e-mail: oli@rses.anu.edu.au, malcolm@rses.anu.edu.au)

(Received March 11, 1997; revised August 12, 1997; accepted August 28, 1997.)